# Autonomous Load Sharing of Voltage Source Converters

Charles K. Sao, *Student Member, IEEE,* and Peter W. Lehn, *Member, IEEE*

***Abstract*—An autonomous load-sharing technique for parallel connected three-phase voltage source converters is presented. An improved power-frequency droop scheme computes and sets the phase angle of the voltage source converter (VSC) directly to yield more rapid real power sharing without sacrificing frequency regulation. Reactive power sharing in the presence of a mismatch between the VSC output interface inductors is achieved by having each VSC regulate the high side voltage with a drooped voltage reference. Dynamics of the reactive power control can be tuned without interfering with steady-state reactive power sharing. Simulation results that validate the proposed technique are also provided.**

***Index Terms*—Load sharing, parallel operation, voltage source converter.**

## I. Introduction

A distributed power system is an electric power distribution network in which power generation and storage resources are widely distributed throughout the network. Typical modern distributed generators do not generate 60-Hz ac voltages and therefore require voltage source converters (VSCs) as part of the circuitry to interface them with the power network. When several such generators are installed on the same network, the VSCs operate in parallel to supply the common loads.

To realize a distributed network with high reliability, the parallel-connected VSCs must share a common load in the absence of the utility supply without exchanging control information among themselves. The real and reactive power controls must operate independently of each other and share a common real and reactive load in proportion to a pre-determined ratio, regardless of plant parameters [1]. Two important classes of autonomous load-sharing techniques that have been proposed to date are the frequency/voltage droop technique, and the signal injection technique.

Though the conventional frequency/voltage droop technique shares a common active load, its reactive power control scheme is plant parameter dependent and does not share reactive power unless the VSCs have perfectly matched output inductors [2]. The signal injection technique proposed by Tuladhar *et al.* overcomes this limitation by having each VSC inject a non-60-Hz signal and use it as a means of sharing a common load with other VSCs on the network [3]. However, the circuitry required to measure the small real power output variations due to the injected signal adds to the complexity of the control.

Manuscript received July 22, 2003; revised October 9, 2003. Paper no. TPWRD-00371-2003.

The authors are with the Department of Electrical and Computer Engineering, University of Toronto, Toronto, ON M5S 3G4, Canada (e-mail: cksao@ ieee.org).

Digital Object Identifier 10.1109/TPWRD.2004.838638

This paper applies the insights gained from a detailed study of conventional droop techniques to propose a new reactive power sharing scheme. The new scheme ensures that VSCs on a distributed power network share a common reactive load regardless of their interface reactance. Additionally, the paper presents an improved real power sharing scheme, which allows the operator to tune its speed of response without sacrificing frequency regulation. Guidelines for tuning the proposed real and reactive power controllers and their stable operating range are also given.

Section II of the paper reviews the system structure while Section III presents a block diagram analysis of VSCs with conventional droop load-sharing control. Section IV proposes an improved version of the frequency droop real power sharing control. The information obtained from the analysis of Section III is employed in Section V to synthesize a novel reactive power sharing scheme. Time domain circuit simulation results are presented and discussed in Section VI. Section VII presents a small-signal stability analysis of the proposed control system.

## II. System Structure

This section describes the network configuration in which the VSCs operate. The VSCs in Fig. 1 can be considered a subset of the distributed power network. They are modeled as voltage sources and are connected to the load bus via interface inductors $L_1$ and $L_2$ and relatively short distribution lines with line impedances $Z_{\text{line1}}$ and $Z_{\text{line2}}$.

The interface inductors make the VSCs less sensitive to disturbances on the load bus [4]. The transfer impedance between each VSC and the load bus is made up of the line impedance and the reactance of the interface inductor. The interface inductors on a distributed power network usually have significantly different reactances.

## III. Analysis of the Conventional Frequency/Voltage Droop Technique

A VSC equipped with the conventional frequency droop scheme autonomously shares a common active load with other VSCs on the network by drooping the frequency of its output voltage as a function of its real power output [2]. It also attempts to share the reactive load by drooping its output voltage magnitude against its reactive power output. These concepts are taken directly from load-sharing control of conventional synchronous generators [5].

### A. Real Power Control

Two VSCs connected to a common load bus are shown in Fig. 1. To share the common active load, the real power sharing

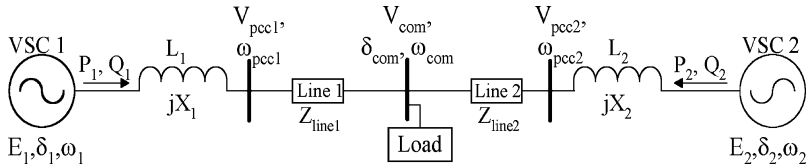


Fig. 1. Two VSCs and a common load.

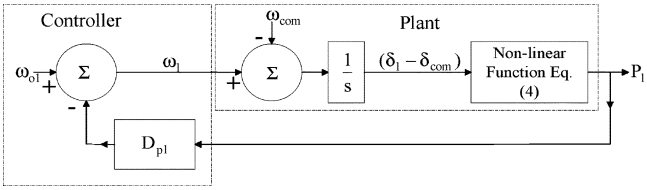


Fig. 2. Large-signal representation of the real power control with conventional frequency droop mechanism.

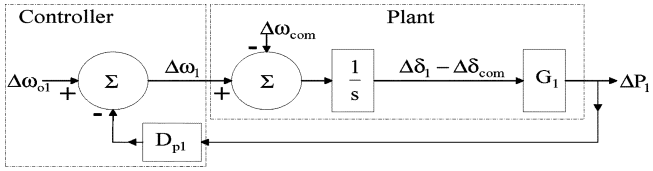


Fig. 3. Small-signal representation of the real power control with conventional frequency droop mechanism.

controllers droop the angular frequencies, $\omega_1$ and $\omega_2$, against the real power outputs, $P_1$ and $P_2$, according to the following control laws:

$$\omega_1 = \omega_{01} - D_{p1}P_1 \tag{1}$$

$$\omega_2 = \omega_{02} - D_{p2}P_2 \tag{2}$$

where $\omega_{01}$ and $\omega_{02}$ are the angular frequency references and $D_{p1}$ and $D_{p2}$ are the frequency droop coefficients.

Analysis begins by studying the operation of VSC 1 delivering power to the common load bus. For the sake of simplicity, the load voltage magnitude is assumed to be fixed. This assumption is valid since the effect of slight load voltage variation on the real power flow is negligible. Moreover, the magnitude of line impedance ($|Z_{\text{line1}}|$) is assumed to be much smaller than the magnitude of the interface impedance ($|jX_1|$).

The control law given by (1) sets the angular frequency $\omega_1$ of the VSC output voltage as a function of the real power $P_1$. The plant, which consists of the VSC and load bus, integrates the difference between the angular frequencies of the VSC and the load bus $(\omega_1 - \omega_{\text{com}})$ over time as per (3). This results in the voltage phase angle difference $(\delta_1 - \delta_{\text{com}})$ across the interface inductor $L_1$. The relation between the real power output, $P_1$, of VSC 1 and its phase angle, $\delta_1$, is given by (4) as

$$(\delta_1 - \delta_{\text{com}}) = \int (\omega_1 - \omega_{\text{com}})dt \tag{3}$$

$$P_1 = \frac{E_1 V_{\text{com}} \sin(\delta_1 - \delta_{\text{com}})}{X_1} \tag{4}$$

where

$E_1$ magnitude of the VSC output voltage;
$V_{\text{com}}$ magnitude of the infinite bus voltage;
$X_1$ interface reactance.

The block diagram of Fig. 2 represents a large-signal model of the real power control and it may be synthesized from (1), (3), and (4). In the diagram, the angular frequency $(\omega_1)$ serves as a control input to the nonlinear plant, which also receives the load bus angular frequency $(\omega_{\text{com}})$ as an input, and generates the output real power $(P_1)$. When the system reaches a stable operating point, the input to the integrator is zero and thus the phase angle difference $(\delta_1 - \delta_{\text{com}})$ and the real power $(P_1)$ remain constant. This condition is achieved only if the angular frequencies $\omega_1$ and $\omega_{\text{com}}$ are equal. Therefore, the real power $(P_1)$ is

$$P_1 = \frac{\omega_{01} - \omega_{\text{com}}}{D_{p1}}. \tag{5}$$

It can be noted that $P_1$ is a linear function of $\omega_{01}$, which may be considered a local reference signal, and $\omega_{\text{com}}$, a remote reference signal. The steady-state gain is the reciprocal of $D_{p1}$, which is a control parameter. Network parameters, such as the interface reactance, do not influence steady-state power flow.

Raising the local frequency reference by applying a positive change to $\omega_{01}$ in (5) results in increased power output. Conversely, the power output can also be raised by lowering the remote frequency reference $\omega_{\text{com}}$. This is the mechanism by which VSC 2 may remotely adjust the output power of VSC 1 in the two VSC system of Fig. 1.

In order to study the dynamics of the system using classical control system analysis tools, a small-signal model is synthesized by linearizing (1), (3), and (4) at an operating point $P_{1i}$, $\delta_{1i}$, $\delta_{\text{comi}}$, $E_{1i}$, and $V_{\text{comi}}$ to yield

$$\Delta\omega_1 = \Delta\omega_{01} - D_{p1}\Delta P_1 \tag{6}$$

$$(\Delta\delta_1 - \Delta\delta_{\text{com}}) = \int (\Delta\omega_1 - \Delta\omega_{\text{com}})dt \tag{7}$$

$$\Delta P_1 = G_1(\Delta\delta_1 - \Delta\delta_{\text{com}}) \tag{8}$$

where

$$G_1 = \frac{E_{1i} V_{\text{comi}} \cos(\delta_{1i} - \delta_{\text{comi}})}{X_1}. \tag{9}$$

Fig. 3 shows a block diagram representing the small-signal model. Deriving the closed-loop transfer functions relating the output $\Delta P_1$ to inputs $\Delta\omega_{01}$, and $\Delta\omega_{\text{com}}$, yields an expression for $\Delta P_1$, as follows:

$$\Delta P_1(s) = \frac{G_1}{s + D_{p1}G_1}\Delta\omega_{01}(s) - \frac{G_1}{s + D_{p1}G_1}\Delta\omega_{\text{com}}(s). \tag{10}$$

It follows from (10) that the eigenvalue of the linearized closed-loop system is

$$\lambda = -D_{p1}G_1. \tag{11}$$

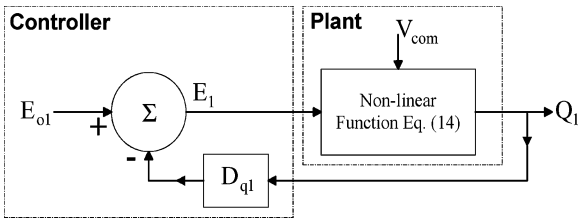


Fig. 4. Large-signal representation of the reactive power control with conventional voltage droop mechanism.

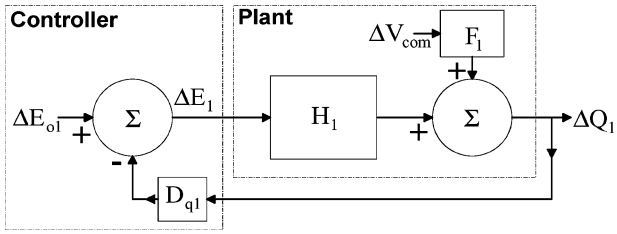


Fig. 5. Small-signal representation of the reactive power control with conventional voltage droop mechanism.

Equation (11) shows that the eigenvalue of the closed-loop system depends on network parameters, the linearization point and on control parameter $D_{p1}$. Thus, $D_{p1}$ is the only available control parameter and it influences both the closed-loop eigenvalue and the steady-state frequency regulation. This makes it impossible to achieve the desired dynamics without compromising frequency regulation. The improved frequency droop scheme presented in Section IV addresses this limitation.

### *B. The Reactive Power Control*

As an attempt to share reactive power, the output voltage magnitudes, $E_1$ and $E_2$, of the two VSCs in Fig. 1 are drooped as functions of the respective reactive power outputs, $Q_1$ and $Q_2$, according to the following control laws:

$$E_1 = E_{01} - D_{q1}Q_1 \tag{12}$$
$$E_2 = E_{02} - D_{q2}Q_2 \tag{13}$$

where $E_{01}$ and $E_{02}$ are the voltage magnitude references and $D_{q1}$ and $D_{q2}$ are the voltage droop coefficients [2].

To understand the reactive power control, the operation of VSC 1, which is delivering reactive power to the common load bus, is analyzed in detail. The load voltage angle is assumed to be fixed. This assumption is valid since the effect of slight angle variation on the reactive power flow is negligible. Moreover, the magnitude of line impedance ($|Z_{\text{line1}}|$) is assumed to be much smaller than the magnitude of the interface impedance ($|jX_1|$).

The control law, given by (12), sets the magnitude $E_1$ of the VSC output voltage as a function of the reactive power output $Q_1$. (14) gives the relation between the voltage magnitude ($E_1$) of VSC 1 and the output reactive power ($Q_1$)

$$Q_1 = \frac{E_1^2 - E_1 V_{\text{com}} \cos(\delta_1 - \delta_{\text{com}})}{X_1}. \tag{14}$$

The block diagram of Fig. 4 represents a large-signal model of the reactive power control and it may be synthesized from (12) and (14). In the diagram, the VSC output voltage magnitude ($E_1$) serves as a control input to the nonlinear plant, which also receives the load bus voltage magnitude ($V_{\text{com}}$) as an input, and generates the output reactive power ($Q_1$). The steady-state solution of the large-signal reactive power control satisfies both (12) and (14) and is given by

$$Q_1 = \frac{-B \pm \sqrt{B^2 - 4\left(E_{01}^2 - NE_{01}\right)D_{q1}^2}}{2D_{q1}^2} \tag{15}$$

where

$$B = ND_{q1} - 2D_{q1}E_{01} - X_1 \tag{16}$$
$$N = V_{\text{com}} \cos(\delta_1 - \delta_{\text{com}}). \tag{17}$$

Solution (15) is nonlinear and depends on not only droop control parameters $E_{01}$ and $D_{q1}$ but also on plant parameters ($V_{\text{com}}$, $\delta_{\text{com}}$, $X_1$) as well as the phase angle $\delta_1$, which is under the control of the real power sharing scheme.

To study the system further, a small-signal model is synthesized by linearizing (12) and (14) at an operating point $Q_{1i}$, $E_{1i}$, $V_{\text{comi}}$, $\delta_{1i}$, and $\delta_{\text{comi}}$ to yield

$$\Delta E_1(s) = \Delta E_{01}(s) - D_{q1}\Delta Q_1(s) \tag{18}$$
$$\Delta Q_1(s) = F_1 \Delta V_{\text{com}}(s) + H_1 \Delta E_1(s) \tag{19}$$

where

$$F_1 = -\frac{E_{1i}\cos(\delta_{1i} - \delta_{\text{comi}})}{X_1} \tag{20}$$
$$H_1 = \frac{2E_{1i} - V_{\text{comi}}\cos(\delta_{1i} - \delta_{\text{comi}})}{X_1}. \tag{21}$$

Fig. 5 shows a block diagram representing the small-signal model. By deriving the closed-loop transfer functions relating the output $\Delta Q_1$ to inputs $\Delta E_{01}$ and $\Delta V_{\text{com}}$, a linearized expression for $\Delta Q_1$ is obtained

$$\Delta Q_1(s) = \frac{H_1}{1 + D_{q1}H_1}\Delta E_{01}(s) + \frac{F_1}{1 + D_{q1}H_1}\Delta V_{\text{com}}(s). \tag{22}$$

It can be seen that the small-signal voltage reference ($\Delta E_{01}$) in (22) can serve as a local reference signal while the disturbance $\Delta V_{\text{com}}$ can be considered a remote reference signal. However, (22) is not plant independent since the coefficients $F_1$ and $H_1$ are functions of the VSC output interface reactance, the linearization point, and $\delta_1$.

### *C. Objectives for New Real Power Sharing Scheme*

The new real power-sharing scheme must have a control parameter that specifies the closed-loop dynamics but does not influence steady-state frequency regulation and other performance metrics.

### *D. Objectives for New Reactive Power Sharing Scheme*

The steady-state solution of the large-signal real power control in (5) is a linear combination of local and remote reference signals with network-independent coefficients. In contrast, the

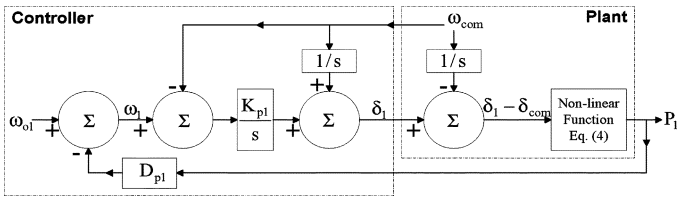


Fig. 6. Large-signal representation of the proposed real power control.

steady-state solution of the large-signal reactive power control, given by (15), is not a linear function of two reference signals.

Like the small-signal real power, the small-signal reactive power is a linear function of two reference signals. However, it is dependent on the phase angle $\delta_1$, which is under the control of the real power-sharing scheme. Hence, it can be said that the reactive power control cannot operate independently of the real power control.

The above observations lead to the following broad control objectives that the proposed reactive power sharing scheme must meet.

1) The steady-state solution must be a linear function of a local reference signal and a remote reference signal.
2) The coefficient(s) in this expression for steady-state reactive power should be independent of network parameters.
3) There should be a control parameter that specifies the closed-loop dynamics but does not influence steady-state voltage regulation, reactive current sharing, or other performance metrics.

## IV. The Proposed Real Power-Sharing Scheme

T his section describes a modified real power sharing scheme for VSC applications. Simulations results are also provided to demonstrate its performance.

### A. Description

In the conventional frequency droop control of generators with speed governors, an integral relation exists between the angular frequency $(\omega_1)$ and phase angle $(\delta_1)$. This is imposed by the physical relation between a generator's speed and its rotor position. No such relation need exist in a VSC-controlled source, though it is typically convenient to emulate such a relation through control action.

Just like the conventional frequency droop power control, the proposed VSC control of Fig. 6 calculates the desired angular frequency $(\omega_1)$ according to the control law cited in (1). However, instead of specifying a reference frequency $(\omega_1)$ for the inherent generator dynamics to integrate with a fixed integrator gain of unity, as shown in Fig. 2, this scheme directly specifies the phase angle $(\delta_1)$ using

$$(\delta_1 - \delta_{\rm com}) = K_{p1} \int (\omega_1 - \omega_{\rm com}) dt. \tag{23}$$

Indeed, (23) is an integral controller that regulates $\omega_{\rm com}$ to track the angular frequency reference $(\omega_1)$. As before, the output $P_1$ of the nonlinear plant depends on the difference between $\delta_1$ and $\delta_{\rm com}$ as per (4). Moreover, the steady-state solution for this real power control is identical to (5).

TABLE I
Plant Parameters for All of the Simulation Cases

| Parameters | VSC 1 | VSC 2 |
|---|---|---|
| Rated Capacity (kVA) | 5 | 5 |
| Rated Capacity ($V_{LL}$) | 115 | 115 |
| Interface Reactance ($\Omega$) | j0.1010 | j0.123 |

TABLE II
Controller Parameters for the Base Case

| Parameters | VSC 1 | VSC 2 |
|---|---|---|
| Angular Freq. Reference ($\omega_0$) in rad/s | 377.045 | 377.045 |
| Freq. Droop Coefficient ($D_p$) in rads/s/kW | 0.018 | 0.018 |
| P Loop Integrator Gain ($K_p$) | 1 | 1 |
| Voltage Magnitude ($E$) in $V_{LL}$ | 112 | 112 |
| Initial Phase Angle ($\delta(0)$) in rad | 0.112 | 0.1 |

The small-signal dynamics are obtained by linearizing equations (1), (4), and (23) and the small-signal real power is

$$\Delta P_1(s) = \frac{K_{p1}G_1}{s + K_{p1}D_{p1}G_1}\Delta\omega_{01}(s) - \frac{K_{p1}G_1}{s + K_{p1}D_{p1}G_1}\Delta\omega_{\rm com}(s). \tag{24}$$

It follows from (24) that the eigenvalue of the linearized closed-loop system is

$$\lambda = -K_{p1}D_{p1}G_1. \tag{25}$$

The above equation shows that the closed-loop system response now depends on the product of the frequency droop coefficient $(D_{p1})$ and the integral gain $(K_{p1})$. Thus, the proposed structure allows the real power control of the VSC to achieve the desired speed of response by varying $(K_{p1})$ without compromising frequency regulation(set by $D_{p1}$). Since direct manipulation of the phase angle $(\delta_1)$ is not possible for generators with conventional speed governors, the proposed real power control is applicable to VSCs only.

Equation (25) also implies that the system is small-signal stable for all operating points at which $(\delta_{1i} - \delta_{\rm comi})$ is between $\pm 90$ degrees if $K_{p1}$ and $D_{p1}$ are positive and dynamic coupling between the real and reactive power controls is neglected.

### B. Simulation

Simulation of the circuit depicted in Fig. 1 is employed to demonstrate large-signal stability and steady-state performance of the proposed real power-sharing scheme. The plant parameters are listed in Table I whereas Table II specifies some relevant controller parameters. The large-signal models of the two VSCs and the real power control are simulated in Simulink. For convenience, the two VSCs are chosen to have equal kVA ratings, although the interface reactors differ.

One benchmark parameter for evaluating performance is the settling time, which in this case is defined as the time it takes for the real power output to converge within 0.2% of the rated output. The other parameter is the circulating power in steady state, which is defined as the difference between the real power

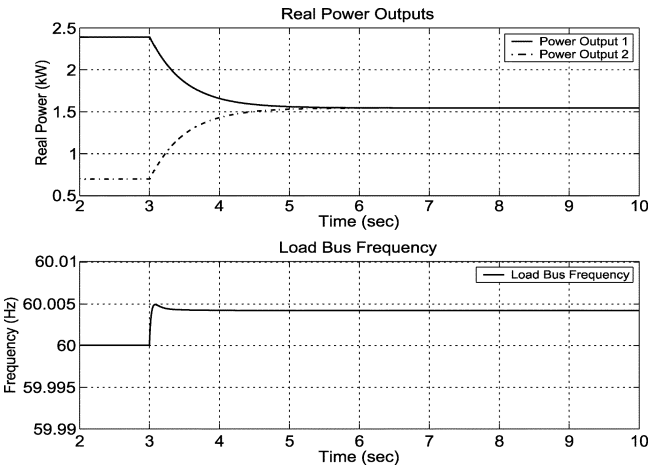


Fig. 7. Dynamic response of the real power control.

TABLE III
EFFECT OF DROOP COEFFICIENT ON SETTLING TIME ($K_p = 1$)

| Droop Coeff. (rad/s/kW) | .0045 | .009 | .018 | .036 | .072 |
|---|---|---|---|---|---|
| Gain x Droop | .0045 | .009 | .018 | .036 | .072 |
| Settling Time (s) | 10.19 | 5.1 | 2.55 | 1.26 | .635 |
| Circulating Power (W) | 0 | 0 | 0 | 0 | 0 |

TABLE IV
EFFECT OF INTEGRATOR GAIN ON SETTLING TIME ($D_p = 0.018$ rad/s/kW)

| Integrator Gain | 0.25 | 0.5 | 1 | 2 | 4 |
|---|---|---|---|---|---|
| Gain x Droop | .0045 | .009 | .018 | .036 | .072 |
| Settling Time (s) | 10.18 | 5.11 | 2.55 | 1.27 | .636 |
| Circulating Power (W) | 0 | 0 | 0 | 0 | 0 |

delivered by the two VSCs. Fig. 7 shows the results of simulating the large-signal models of the two VSCs in Fig. 1 assuming that they are initially generating unequal powers. It can be seen that there is no circulating real power in steady state and that the settling time is 2.55 s. The load bus frequency, which is designed to be exactly 60 Hz at half load, rises as the load is only 30% of the combined VSC rating.

As the VSCs cannot measure $\omega_{\rm com}$ locally when the line impedances are included in the model, they use the angular frequencies at the points of common coupling ($\omega_{pcc1}$ and $\omega_{pcc2}$) as the feedback signals to compute the output voltage phase angles as per (23). However, (5) remains valid and the VSCs share real power because both $\omega_{pcc1}$ and $\omega_{pcc2}$ are equal to $\omega_{\rm com}$ in steady state.

The simulation is repeated with a number of different frequency droop coefficients ($D_p$) and integrator gains ($K_p$) to study the effect of these parameters on the speed of response and load-sharing accuracy. Table III presents the results of a set of simulations in which the integrator gain is fixed at 1 and the droop coefficient is varied. The case is also simulated with different integrator gains while fixing the droop coefficient at 0.018 rad/s/kW. The results are shown in Table IV.

The results in Tables III and IV show that there is no circulating real power between the two VSCs in steady state and that the speed of convergence depends on the product of the droop coefficient and the integrator gain as anticipated.

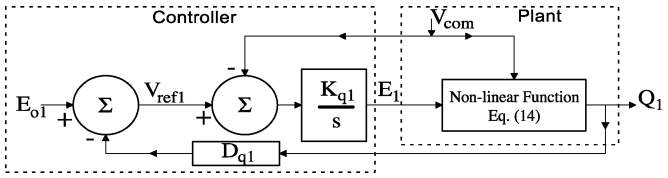


Fig. 8. Large-signal representation of the proposed reactive power control.

Thus, the procedure for tuning the real power control loops of a group of parallel VSCs for optimal speed of response without compromising the frequency regulation is as follows.

1) Determine the desired speed of response. While, it should be faster than the slowest acceptable speed of response, the control loop should not be faster than the dynamics of the power source or any underlying converter controls.
2) Fix the droop coefficient ($D_p$) to meet the frequency regulation requirement.
3) Vary the integrator gain ($K_p$) to achieve desired system response, as specified in step 1.

## V. PROPOSED REACTIVE POWER-SHARING SCHEME

This section proposes a reactive power-sharing scheme that shares a common reactive load regardless of plant parameters.

### A. Description

The block diagram of Fig. 8 is the large-signal model of the proposed reactive power control. As in the conventional voltage droop scheme, the VSC output voltage magnitude ($E_1$) serves as a control input to the nonlinear plant, which also receives the load bus voltage magnitude ($V_{\rm com}$) as an input, and generates the output ($Q_1$). However, the control input $E_1$ in the proposed scheme is generated by an integral controller that regulates $V_{\rm com}$ to track a reference $V_{\rm ref1}$. The reference is drooped against the reactive power output $Q_1$. These control laws can be stated mathematically as

$$E_1 = K_{q1} \int (V_{\rm ref1} - V_{\rm com}) dt \tag{26}$$

$$V_{\rm ref1} = E_{01} - D_{q1} Q_1. \tag{27}$$

This scheme shows resemblance to the high side-voltage control in some large power plants [6]. Assuming stability, the input to the integrator will be zero when the system reaches steady state. Thus, equating $V_{\rm ref1}$ to $V_{\rm com}$ in (27) yields the steady-state reactive power relation

$$Q_1 = \frac{E_{01} - V_{\rm com}}{D_{q1}}. \tag{28}$$

It can be noted that $Q_1$ is now a linear function of a local reference signal, namely $E_{01}$, and a remote reference signal, $V_{\rm com}$. The steady-state gain is the reciprocal of $D_{q1}$, which is a control parameter. Network parameters, such as the interface reactance, no longer influence steady-state reactive power flow.

When employing the proposed reactive power sharing scheme to control the two VSCs in Fig. 1, $Q_1$ is given by (28) and the expression for $Q_2$ is given by (29). Provided that the local references ($E_{01}$ and $E_{02}$) are identical, the droop

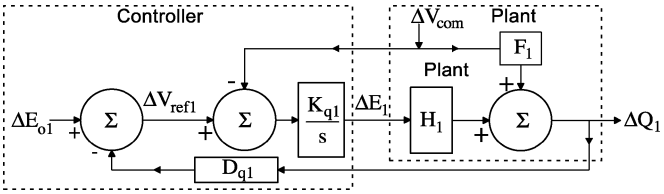


Fig. 9. Small-signal representation of the proposed reactive power control.

coefficients determine the reactive load distribution between the two VSCs according to (30)

$$Q_2 = \frac{E_{02} - V_{\rm com}}{D_{q2}} \tag{29}$$

$$\frac{Q_1}{Q_2} = \frac{D_{q2}}{D_{q1}}. \tag{30}$$

In order to study the dynamics of the system, a small-signal model is synthesized by linearizing (26) and (27) at an operating point $Q_{1i}$, $E_{1i}$, $V_{\rm com}$, $\delta_{1i}$, and $\delta_{\rm comi}$ to yield

$$\Delta E = K_{q1} \int (\Delta V_{\rm ref1} - \Delta V_{\rm com}) dt \tag{31}$$

$$\Delta V_{\rm ref1} = \Delta E_{01} - D_{q1} \Delta Q_1. \tag{32}$$

The linearized plant model given by (19) remains valid. Fig. 9 shows a block diagram representing the complete small-signal model with controller. The closed-loop transfer function relating the output $\Delta Q_1$ to $\Delta E_{01}$ and $\Delta V_{\rm com}$ in the block diagram is given by (33)

$$\Delta Q_1(s) = \frac{K_{q1} H_1}{s + K_{q1} D_{q1} H_1} \Delta E_{01}(s) + \frac{sF_1 - K_{q1} H_1}{s + K_{q1} D_{q1} H_1} \Delta V_{\rm com}(s). \tag{33}$$

The above equation shows that the closed-loop eigenvalue of the linearized system is

$$\lambda = -K_{q1} D_{q1} H_1. \tag{34}$$

Equation (34) shows that the eigenvalue of the closed-loop system depends on the product of $K_{q1}$ and $D_{q1}$, which alone influences the steady-state voltage regulation. Having $K_{q1}$ as a control parameter allows the reactive power control to achieve the desired dynamics without affecting voltage regulation.

It also follows from (34) that the system with positive values of $D_{q1}$ and $K_{q1}$ is small-signal stable for all operating points at which $(V_{\rm comi} \cos(\delta_{1i} - \delta_{\rm comi}))$ is less than twice the value of $E_1$; this is always the case for power systems under normal operation. This statement is valid if dynamic coupling between the P and Q controls is neglected.

### *B. Simulation Neglecting Line Impedance*

This simulation study is to demonstrate large-signal stability and steady-state performance of the proposed reactive power-sharing scheme when the line impedances are negligible compared to the VSC interface reactances. The same simulation case of Fig. 1 is employed and relevant controller parameters are included in Table V. The large-signal model of the two VSCs and the reactive power control is simulated in Simulink.

TABLE V
PARAMETERS FOR THE BASE CASE

| Parameters | VSC 1 | VSC 2 |
|---|---|---|
| Load Bus Voltage Reference ($E_0$) in $V_{LL}$ | 110.25 | 110.25 |
| Voltage Droop Coefficient ($D_q$) in V/kVAr | 0.1 | 0.1 |
| Q Loop Integrator Gain ($K_q$) | 10 | 10 |
| Phase Angle ($\delta$) in rad | 0 | 0 |
| Initial Voltage Magnitude($E(0)$) in $V_{LL}$ | 109.75 | 111.7 |

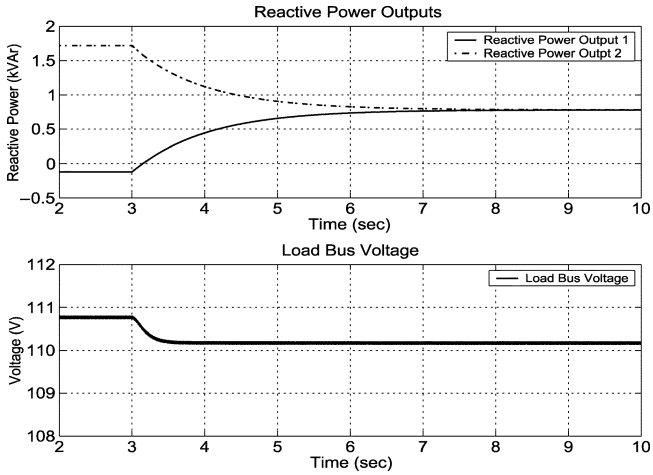


Fig. 10. Dynamic response of the reactive power control.

TABLE VI
EFFECT OF DROOP COEFFICIENT ON SETTLING TIME ($K_q = 10$)

| Droop Coeff. (V/kVAr) | 0.025 | 0.05 | 0.1 | 0.2 | 0.4 |
|---|---|---|---|---|---|
| Gain x Droop | 0.25 | 0.5 | 1 | 2 | 4 |
| Settling Time (s) | 20.8 | 10.4 | 5.22 | 2.6 | 1.3 |
| Circulating Power (VAr) | 0 | 0 | 0 | 0 | 0 |

TABLE VII
EFFECT OF INTEGRATOR GAIN ON SETTLING TIME ($D_q = 0.1$ V/kVAr)

| Integrator Gain | 2.5 | 5 | 10 | 20 | 40 |
|---|---|---|---|---|---|
| Gain x Droop | 0.25 | 0.5 | 1 | 2 | 4 |
| Settling Time (s) | 20.8 | 10.4 | 5.22 | 2.6 | 1.3 |
| Circulating Power (VAr) | 0 | 0 | 0 | 0 | 0 |

Fig. 10 shows the simulation results. It can be seen that there is no circulating reactive power in steady state. The time for the reactive powers to settle within 0.2% of rated output is 5.22 s. The load bus voltage, which is designed to be exactly 110 V at half load, drops to 110.17 V as the load is 15.64% of the combined VSC rating.

The simulation is repeated with a number of different voltage droop coefficients $(D_q)$ and integrator gains $(K_q)$ to study the effect of these parameters on the speed of response and load-sharing accuracy. Table VI presents the results of a set of simulations in which the integrator gain is fixed at 10 and the droop coefficient is varied. The case is also simulated with different integrator gains while fixing the droop coefficient at 0.1 V/kVAr. The results are shown in Table VII.

The results in Tables VI and VII show that, despite mismatched VSC interface reactances, there is no circulating reactive power between the two VSCs in steady state and that the speed of convergence depends on the product of the droop coefficient and the integrator gain.

TABLE VIII
EFFECT OF DROOP COEFFICIENT ON SETTLING TIME ($K_q = 10$)

| Droop Coeff.(V/kVAr) | 0.025 | 0.05 | 0.1 | 0.2 | 0.4 |
|---|---|---|---|---|---|
| Gain x Droop | 0.25 | 0.5 | 1 | 2 | 4 |
| Circulating VAr | 156.9 | 104.8 | 62.9 | 34.9 | 18.5 |

TABLE IX
EFFECT OF INTEGRATOR GAIN ON SETTLING TIME ($D_q = 0.1$ V/kVAr)

| Integrator Gain | 2.5 | 5 | 10 | 20 | 40 |
|---|---|---|---|---|---|
| Gain x Droop | 0.25 | 0.5 | 1 | 2 | 4 |
| Circulating VAr | 62.9 | 62.9 | 62.9 | 62.9 | 62.9 |

### C. Simulation With Line Impedances

While the proposed reactive power sharing is immune to mismatched VSC interface reactance values, it does not compensate for line impedance mismatches. However, the circulating reactive power will remain insignificant if the line impedances are small compared to the output impedances of the VSCs. The aim of this simulation case is to study the effect of the voltage droop coefficient and the integrator gain on the amount of circulating reactive power in steady state. In order to do so, the line impedances shown in Fig. 1 are now included in the simulation. The values of $Z_{\text{line1}}$ and $Z_{\text{line2}}$ are j0.002 26 and j0.003 39 $\Omega$, respectively. Other circuit and control parameters remain as they are in the simulation case of the previous subsection.

As previously, the simulation is repeated with a number of different voltage droop coefficients $(D_q)$ and integrator gains $(K_q)$ to study the effect of these parameters on the load-sharing accuracy. Results are summarized in Tables VIII and IX.

The presence of the steady-state circulating reactive power may be explained as follows. With the line impedances included, the VSCs cannot measure $V_{\text{com}}$ locally, and therefore use the voltages at the points of common coupling ($V_{pcc1}$ and $V_{pcc2}$) as the feedback signals to compute the output voltage magnitudes as per (26). Since $V_{\text{com}}$, $V_{pcc1}$, and $V_{pcc2}$ are not equal in steady state, the two VSCs do not have a common remote reference signal to ensure that they share the common reactive load.

The results also show that the integrator gain has no influence on the steady-state circulating reactive power in the network. The only control parameter that influences circulating reactive power is the voltage droop coefficient. Having a high droop coefficient, and hence compromising voltage regulation, results in lower circulating power. *Thus, when tuning the reactive power control, selecting the voltage droop is a tradeoff between the load-sharing accuracy and voltage regulation.*

The procedure for tuning the reactive power control loops of a group of parallel VSCs for optimal speed of response in the presence of significant line impedance is as follows.

1) Determine the desired speed of response. While, it should be faster than the slowest acceptable speed of response, the control loop should be significantly slower than any underlying voltage controls.
2) Determine the allowable circulating reactive power.
3) Fix the droop coefficient $(D_q)$ to meet both the voltage regulation and circulating power requirements. Note that increasing the VSC interface reactor size or adjusting the values of $E_{01}$ and $E_{02}$ would also reduce the circulating reactive power.
4) Vary the integrator gain $(K_q)$ to achieve the desired system response, as specified in step 1.

## VI. EFFECT OF REAL AND REACTIVE POWER CONTROL CROSS-COUPLING ON STABILITY

The simplified eigenvalue analyzes in Sections IV and V are adequate for computing speeds of response of the real and reactive power controls. However, they provide an overly optimistic range for stability as they neglect dynamic coupling between the two controls.

Even assuming a stiff load bus with $\Delta V_{\text{com}} = 0$ and $\Delta\delta_{\text{com}} = 0$, the dependence of $\Delta P_1$ on $\Delta E_1$ and $\Delta Q_1$ on $\Delta\delta_1$ must be taken into account. $\Delta P_1$ and $\Delta Q_1$ are given by

$$\Delta P_1 = G_1\Delta\delta_1 + C_{pe1}\Delta E_1 \tag{35}$$

$$\Delta Q_1 = H_1\Delta E_1 + C_{qd1}\Delta\delta_1 \tag{36}$$

where

$$C_{pe1} = \frac{V_{\text{comi}}\sin(\delta_{1i} - \delta_{\text{comi}})}{X_1} \tag{37}$$

$$C_{qd1} = \frac{E_{1i}V_{\text{comi}}\sin(\delta_{1i} - \delta_{\text{comi}})}{X_1}. \tag{38}$$

Equations (35) and (36) replace (8) and (19) if cross-coupling is to be considered. For typical operating conditions, $C_{pe1} \ll G_1$ and $C_{qd1} \ll H_1$, implying weak coupling between the real and reactive power controls. The dynamics of the coupled real and reactive power controls are given by

$$\begin{bmatrix} \Delta\dot{\delta}_1 \\ \Delta\dot{E}_1 \end{bmatrix} = \begin{bmatrix} -K_{p1}D_{p1}G_1 & -K_{p1}D_{p1}C_{pe1} \\ -K_{q1}D_{q1}C_{qd1} & -K_{q1}D_{q1}H_1 \end{bmatrix} \begin{bmatrix} \Delta\delta_1 \\ \Delta E_1 \end{bmatrix}. \tag{39}$$

It can be demonstrated that the closed-loop eigenvalues are negative if the system satisfies the nonlinear inequality:

$$G_1H_1 > C_{pe1}C_{qd1}. \tag{40}$$

The analytic solution of (40) is

$$\cos(\delta_{1i} - \delta_{\text{comi}}) > \frac{V_{\text{comi}}}{2E_{1i}}. \tag{41}$$

Consequently, the range of phase angle for stable operation depends on the ratio of the magnitude of the VSC output voltage to that of the load bus voltage. When the ratio is 1, the system is small-signal stable for all operating points at which $(\delta_{1i} - \delta_{\text{comi}})$ is between $\pm 60°$. Increasing the ratio by 15% adds 8.4 degrees to the stable operating range while reducing it by 15% shrinks the range by 12°. Thus it may be concluded that the cross-coupling reduces the range of stable operation.

This stability analysis investigates the dynamic interaction of the real and reactive controls of a single converter where this lone converter has a negligible effect on the bus voltage. This would be the case if the load is supplied by many converters. If the VSC under study has a large influence on the load bus voltage, then a complete eigenvalue analysis of the entire system including the load is required.

This is seen as outside the scope of this paper since such an analysis is invariably load specific.

TABLE X
CONTROLLER PARAMETERS FOR THE EMTDC SIMULATION

| Parameters | VSC 1 | VSC 2 |
|---|---|---|
| Angular Freq. Reference ($\omega_0$) in rad/s | 377.045 | 377.045 |
| Freq. Droop Coeff. ($D_p$) in rad/s.kW | 0.018 | 0.018 |
| P Integrator Gain ($K_p$) | 1 | 1 |
| Load Volt. Reference ($E_0$) in $V_{LL}$ | 110.25 | 110.25 |
| Volt. Droop Coeff. ($D_q$) in V/kVAr | 0.1 | 0.1 |
| Q Integrator Gain ($K_q$) | 10 | 10 |
| Initial Volt. Mag. ($E$) in $V_{LL}$ | 112 | 112 |
| Initial Phase Angle ($\delta(0)$) in rad | 0.112 | 0.1 |

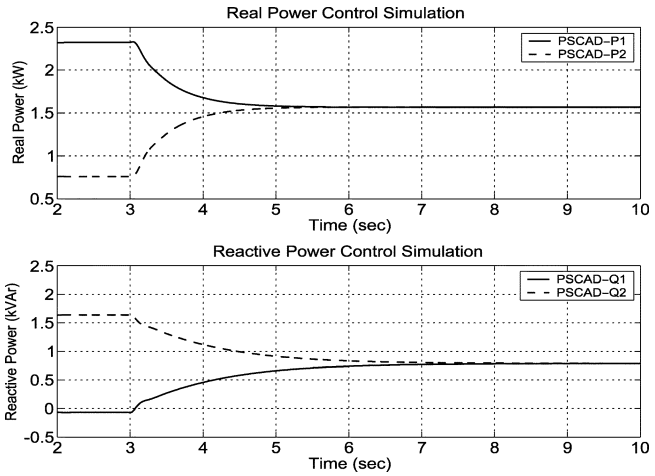


Fig. 11. Dynamic response of the real and reactive power control.

## VII. VSC CIRCUIT SIMULATION AND RESULTS

The VSCs of Fig. 1 are simulated in PSCAD/EMTDC, a time domain circuit simulation tool for power systems. It demonstrates the large-signal stability and steady-state performance of the proposed real and reactive power controllers on two VSCs when both controllers operate simultaneously. It also demonstrates the compatibility of these controllers to the underlying voltage controllers of the VSCs.

For each VSC, its real power control sets the desired angle of the output voltage whereas the reactive power control sets the desired voltage magnitude. These control signals, generated by the power sharing controllers, serve as reference signals for a current regulated voltage controller. The controller takes advantage of an LC filter network at the VSC output and is capable of tracking the magnitude and angle references independently. This PSCAD/EMTDC simulation case includes the voltage controllers, though they will not be described here.

Both the real and reactive power controls are activated simultaneously in this simulation. The control parameters and the initial values of the output voltage magnitudes and phase angles are given in Table X. The effect of line impedances is neglected.

The real and reactive power outputs of the two VSCs in the model are plotted against time in Fig. 11. Initially, the voltages of the VSCs are tracking constant magnitude and angle references and they are not sharing load. The load-sharing controllers are activated at $t = 3$ seconds and the real and reactive power outputs of the two VSCs converge gradually. The settling time for the real power control is 2.55 and that for the reactive power control is 5.22 s.

## VIII. CONCLUSION

This paper focuses on an improvement to the conventional frequency droop scheme for real power sharing and the development of a new reactive power-sharing scheme. The improved frequency droop scheme computes and sets the phase angle of the VSC instead of its frequency. This allows the operator to tune the real power sharing controller to achieve desired system response without compromising frequency regulation.

The proposed reactive power sharing scheme introduces integral control of the load bus voltage, combined with a reference that is drooped against reactive power output. This causes two VSCs on a common load bus to share the reactive load exactly in the presence of mismatched interface inductors if the line impedances are much smaller than the interface reactors. Thus, reactive power sharing is achieved without control interconnections or injecting control signals into the power lines. Moreover, in the proposed reactive power control, the integrator gain can be varied to achieve the desired speed of response without affecting voltage regulation.

## REFERENCES

[1] R. Lasseter and P. Piagi, "Providing premium power through distributed resources," in *Proc. 33rd Hawaii Int. Conf. System Sciences*, Jan. 2000, pp. 1437–1445.
[2] M. C. Chandorkar, D. Divan, and R. Adapa, "Control of parallel connected inverters in standalone ac supply systems," *IEEE Trans. Ind. Applicat.*, vol. 29, pp. 136–143, Jan. 1993.
[3] A. Tuladhar, H. Jin, T. Unger, and K. Mauch, "Control of parallel inverters in distributed ac pouver systems with consideration of the line impedance tifect," in *Proc. APEC*, vol. 1, Feb. 1998, pp. 321–328.
[4] M. C. Chandorkar, D. Divan, Y. Hu, and B. Banerjee, "Novel architectures and control for distributed ups systems," in *Proc JAPEC*, vol. 2, Feb. 1994, pp. 683–689.
[5] J. D. Glover and M. S. Sarma, *Power System Analysis and Design*. Pacific Cove, CA: Books/Cole, 2002.
[6] J. Davies and L. Midford, "High side voltage control at manitoba hydro," in *Proc. IEEE PES Summer Meeting*, vol. 1, July 2000, pp. 271–277.

**Charles K. Sao** (S'01), photograph and biography not available at the time of publication.

**Peter W. Lehn** (M'99), photograph and biography not available at the time of publication.